



OPEN ACCESS

EDITED BY

Di Wang,
University of Ottawa, Canada

REVIEWED BY

Zhenkun Li,
Aalto University, Finland
Xinzhou Li,
Chang'an University, China

*CORRESPONDENCE

Qinghe Lu,
✉ ludustvail@163.com

RECEIVED 22 April 2024

ACCEPTED 16 May 2024

PUBLISHED 12 June 2024

CITATION

Lu Q, Liu X, Lu Z and Li K (2024), Synthesis and characterization of polyurethane-based self-luminous pavement coatings: a performance evaluation study. *Front. Mater.* 11:1421349. doi: 10.3389/fmats.2024.1421349

COPYRIGHT

© 2024 Lu, Liu, Lu and Li. This is an open-access article distributed under the terms of the [Creative Commons Attribution License \(CC BY\)](https://creativecommons.org/licenses/by/4.0/). The use, distribution or reproduction in other forums is permitted, provided the original author(s) and the copyright owner(s) are credited and that the original publication in this journal is cited, in accordance with accepted academic practice. No use, distribution or reproduction is permitted which does not comply with these terms.

Synthesis and characterization of polyurethane-based self-luminous pavement coatings: a performance evaluation study

Qinghe Lu^{1*}, Xiajun Liu², Zhen Lu² and Ke Li^{1,3}

¹Institute of Mining Engineering, Guizhou Institute of Technology, Guiyang, China, ²School of Civil Engineering and Architecture, Guizhou Minzu University, Guiyang, China, ³School of Mining and Mechanical Engineering, Liupanshui Normal University, Shuicheng, China

Improving the nighttime vision of drivers is essential, given the growing advancements in urban transportation. In this study, polyurethane-based self-luminous pavement coatings (PSCs) were prepared by doping luminous powders (LPs) into the polyurethane materials. The superior optical properties and chemical stabilities of these coatings were ensured by synthesizing the polyurethane-based material. Then, the PSCs were evaluated for their comprehensive performances, such as luminescence, aging resistance, and abrasion resistance, using various characterization methods, including fluorescence spectral analysis, Fourier-transform infrared spectroscopy, fluorescence microscopy, and mechanical property testing. The results show that the 50-mesh LP has the optimal overall performance, with an initial luminescence that exceeds those of the 100 and 400 meshes. The initial brightness of the PSC is mainly influenced by the LP and increases with dosage. The lattice structure and luminescent properties of the luminescent material did not change after coating preparation. The peak excitation wavelength of 420 nm implies that the coating has the best excitation effect under UV light. The primer-marking coating effectively improves the abrasion resistance of the PSC, and the mass loss of the PSC with a coating thickness of 0.4 kg/m² is 52.9% of that without the primer-marking coating, with the optimal coating thickness being 0.6 kg/m². This research provides an innovative solution to improve nighttime roadway lighting, which provides useful support for the sustainable development of urban transportation infrastructures and construction of intelligent transportation systems.

KEYWORDS

self-luminous pavement, polyurethane, luminescent property, antiaging property, wear resistance

1 Introduction

In recent times, there has been a significant push toward enhancing the autonomy of road infrastructures with the aim of mitigating their impacts on industrial systems. In this context, the development of a diverse array of intelligent roadways has garnered considerable attention from the research community. Innovations such as self-temperature

regulation, self-luminous pavements (SLPs), self-sustaining energy supplies, and eco-friendly construction materials have progressively been highlighted (Sha et al., 2021; Dong et al., 2023). In particular, the emergence of SLPs is noteworthy as these are engineered to efficiently store and convert light energy. During daylight hours, these pavements absorb solar radiation and subsequently exhibit active light-emitting function at night. This novel feature effectively diminishes the reliance on electrical power for nocturnal illumination, thereby enhancing the self-sufficiency and economic viability of road lighting systems significantly (Wang et al., 2022a; Wang W. et al., 2023). Moreover, the deployment of SLP materials can alleviate the adverse effects associated with conventional road lighting, such as light pollution, which can have detrimental impacts on both human health and the ecological environment (Li P. et al., 2023). Furthermore, the implementation of SLPs in road construction reduces the need for external lighting installations, consequently leading to a decrease in the associated construction and post-maintenance expenses (Guo and Liu, 2022). The appeal of SLPs has not gone unnoticed as they have garnered the favor of road construction professionals across various countries. Consequently, researchers are actively engaged in the exploration and development of advanced SLP materials with the goal of redefining the boundaries of possibility in the realm of sustainable and autonomous road infrastructures.

SLP coatings represent a specialized category of luminescent road surfacing that are typically achieved through the application of phosphorescent materials on existing road surfaces to create luminous functional layers (Del Serrone et al., 2023; Pan et al., 2023). These coatings have been recognized for their utility in a range of applications, including road marking, architectural embellishment, landscape enhancement, and the erection of cautionary signages (Walther et al., 2019; Li et al., 2021; Li P. et al., 2023; Okimura et al., 2023; Pan et al., 2023). The luminescent properties of SLP coatings can augment the visibility of road outlines, thereby mitigating the risks associated with vehicular navigation (Li P. et al., 2023; Lin et al., 2023). In terms of formulation, SLP coatings are engineered using polymer resins as the primary film-forming agents and complemented by luminescent materials in a subordinate film-forming role (Wang et al., 2022b; Wang K. et al., 2023; Pan et al., 2023). The optimal performance of such coatings is contingent upon the film-forming substance exhibiting high light transmittance, robust adhesion characteristics, and superior resistance to environmental degradation (Fang et al., 2009). Various resin types are suitable for use as the film-forming materials in self-luminous coatings, with epoxy, acrylic, polyurethane, and fluorine resins being among the most commonly utilized options (Bredol et al., 1991; Poulikakos et al., 2022; Villa et al., 2022). These materials are often selected for their ability to provide durable and effective luminescent layer that can withstand the rigors of outdoor exposure while maintaining the intended functional attributes over an extended period of time.

With regard to luminescent coating materials, numerous research endeavors have been undertaken to optimize their synthesis and performance characteristics. Yuanshuai et al. (2020) formulated luminescent coatings using silicone-modified phenylpropylene emulsion as the primary film-forming agent; through a systematic orthogonal test, they meticulously determined the optimal doping

levels of various components to achieve maximum luminescence brightness. Subsequent evaluations of the luminescent and mechanical properties of these coatings provided valuable insights into the overall performances of the materials. As a complement to this work, Hai et al. (2019) investigated the use of acrylic resin modified with silicone-silica sol as the principal film-forming material for self-luminous coatings; their study delved into the spectral properties and luminescence decay characteristics of the coatings. The findings revealed that both the concentration of luminescent dopants and intensity of the excitation light are critical factors influencing the luminous brightness of the coating. It was observed that increased doping levels and more intense excitation lighting resulted in longer luminous afterglows. Similarly, Gao et al. (2013) employed a pure emulsion as the main film-forming material coupled with 23–38 μm luminescent materials to fabricate luminescent coatings; their research demonstrated that the afterglow durations of these coatings could be extended to over 8 h. One of the interesting observations of their study was that although elevated doping levels enhanced the initial brightness, no further increase in brightness could be achieved once the doping level reached 50%. Expanding on the understanding of luminescent coatings, Lyu et al. (2020) explored the impacts of pore-forming agents on the material's performance; by incorporating fluorine-containing acrylic resins, they successfully developed self-luminous coatings with improved luminescent brightness without compromising the crystalline integrity of the material.

Investigations into the luminescent characteristics of various coatings have been the focus of numerous researchers. Wei et al. (2022) comprehensively studied the efficacies of luminescent coatings, with specific emphasis on epoxy resins as the principal film-forming substances; they meticulously examined the influences of the luminescent material doping levels and particle dimensions on the luminescent properties. The results demonstrated that the developed coatings were capable of emitting light for an extended duration of over 7 h in nocturnal darkness, showcasing their practical utility in low-light environments. In a parallel study, Mierlo (2017) explored the application of luminescent coatings on cobblestones by utilizing polyurethane as the primary film-forming material; this investigation revealed that coatings with luminescent material dopant concentrations exceeding 20% and thicknesses greater than 200 μm exhibited superior luminescent performances. Remarkably, these coatings were able to maintain afterglows for up to 20 h, underscoring their potential in long-term illumination under outdoor settings. Bacero et al. (2015) explored the use of petroleum resin as the main film-forming material in luminescent coatings, and they identified that a dopant concentration of 25% within the luminescent material could yield an afterglow for approximately 8 h.

In the context of pavement luminescence, the fabrication of luminescent coatings is highlighted for its simplicity and efficiency. To further enhance the luminous brightness, the coating formulations typically incorporate colorless and transparent materials as the primary film-forming substances. This strategic choice allows amplification of the inherent light-emitting capabilities of these coatings, ensuring that they maximally effective. Despite these advancements, studies on luminescent coating preparations have predominantly focused on acrylic resins as the main film-forming materials (Falchetto et al., 2018; Bi et al., 2021; Wang K. et al., 2023). There is a relative

paucity of investigations into alternative resin-based materials, including polyurethane-based formulations, which are currently underexplored for road applications. Regarding the application scenarios for luminescent coatings, they are primarily utilized in contexts such as tunnel curtain walls or road markings. In these settings, the primary concern involves evaluation of the adhesion of the film-forming substance to the concrete surface (Falchetto et al., 2018; Praticò et al., 2018; Zheng et al., 2023). However, it is crucial to recognize that coatings deployed for road markings must not only exhibit effective luminescence at night but also possess certain levels of abrasion resistance and load-bearing capacity to withstand the rigors of real-world vehicular traffic and environmental conditions.

Therefore, future research endeavors should aim to diversify the range of film-forming materials considered for luminescent coatings, with particular emphasis on the development of polyurethane-based materials. Additionally, the durability and structural integrity of these coatings under practical conditions must be tested rigorously and optimized to ensure long-term viability and performance in road safety applications. Therefore, the present study involves formulation of polyurethane-based SLP coatings (PSCs) by employing polyurethane as the principal film-forming substance. Additionally, luminous powders (LPs) and reflective powders (RPs) are utilized in a secondary capacity as film formers that contribute to the multifaceted nature of these coatings. This research delves into the intricate design of the material's composition, meticulously assessing its indoor afterglow attributes, resistance to aging, endurance against abrasion, and antipeeling capabilities. This comprehensive evaluation is aimed at optimizing the PSCs to meet the rigorous demands of road infrastructure applications. The findings of this study are anticipated to yield valuable insights and innovative concepts that can inform the design and application processes of SLP materials.

2 Materials and methods

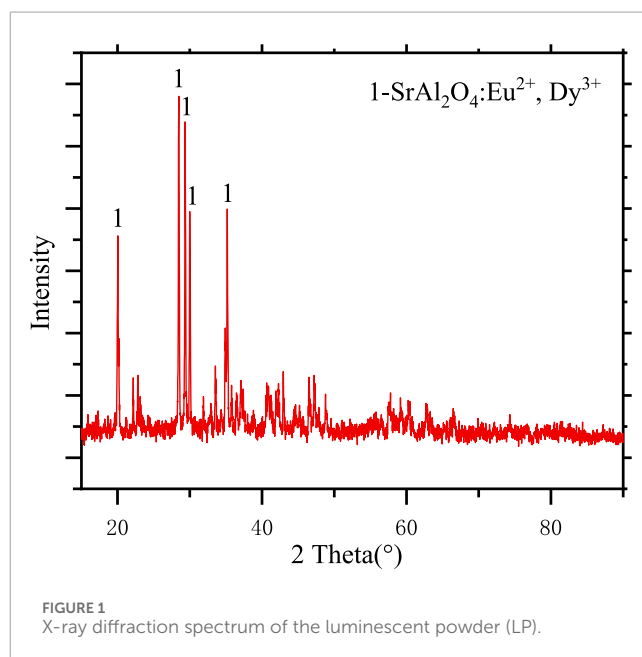
2.1 Raw materials and preparation

2.1.1 Polyurethane

The synthesis of polyurethane is fundamentally based on the reaction between polyisocyanates and polyols, which serve as the key precursors. Given the presence of the benzene ring in its molecular structure, toluene diisocyanate (TDI) is recognized to impart enhanced hardness and resistance to deformation (Sayles et al., 2022; Schupp and Plehiers, 2022). Consequently, TDI and polyester polyol were chosen as the foundational components for the synthesis of polyurethane in this study. It is noteworthy that the finished products of two-component polyurethane systems demonstrate superior performance characteristics, including increased hardness, tensile strength, and tear resistance, compared to their one-component counterparts (Bashir et al., 2022). Hence, two-component polyurethane was selected as the optimal luminescent base material in this investigation. Table 1 lists the conventional physical property indexes of two-component (2:1 ratio of the main agent to curing agent) polyurethanes.

TABLE 1 Physical properties of polyurethane.

Indicator	Results
Appearance at room temperature	Light-yellow translucent thick liquid
Hardness (Shore A)	95 ± 5
Tensile strength (MPa)	73.5
Tear strength (kN/m)	135.6
Tearing elongation (%)	593



2.1.2 Luminous and reflective powders

The LPs and RPs were produced in Hebei Province, China, and the mineral compositions of the LPs were determined by X-ray diffraction (XRD) (Figure 1), which yielded the following main components for $\text{SrAl}_2\text{O}_4: \text{Eu}^{2+}$ and Dy^{3+} . The chemical compositions and specifications of the LPs and RPs are shown in Tables 2 and 3, respectively.

For the purpose of particle size optimization, the representative LP particle sizes in this study were determined to be 50 mesh for coarse particles, 100 mesh for medium particles, and 400 mesh for fine particles. In accordance with the testing protocols outlined in the GB/T 5838.3–2015 standard (phosphor-part 3: performance test techniques), each of the three distinct particle sizes of LPs was subjected to ultraviolet (UV) radiation at a wavelength of 365 nm for 5 min. This exposure was designed to activate the luminescent properties of these particles. A luminance measurement equipment was then used to measure the afterglow intensities, whose findings are displayed in Figure 2.

Figure 2 shows that the initial luminance levels of the LP particles of 50, 100, and 400 meshes were 15.26 cd/m^2 , 13.65 cd/m^2 , and 12.13 cd/m^2 , which decreased to 0.483 cd/m^2 , 0.315 cd/m^2 , and 0.210 cd/m^2 after 2 h, respectively. It is noteworthy that as

TABLE 2 Chemical composition of the 100 mesh (medium sized) LP.

Average particle size (μm)	Chemical composition (%)						
	SrO	Al ₂ O ₃	ZrO ₂	Dy ₂ O ₃	Eu ₂ O ₃	MgO	CaO
100	6.41	87.58	2.69	0.79	0.81	1.25	0.21

TABLE 3 Physical composition of the RP.

Refractive index	Average particle size (μm)	Chemical composition (%)			
		SiO ₂	Na ₂ O	CaO	MgO
2.01	150	70.09	14.18	9.81	4.01

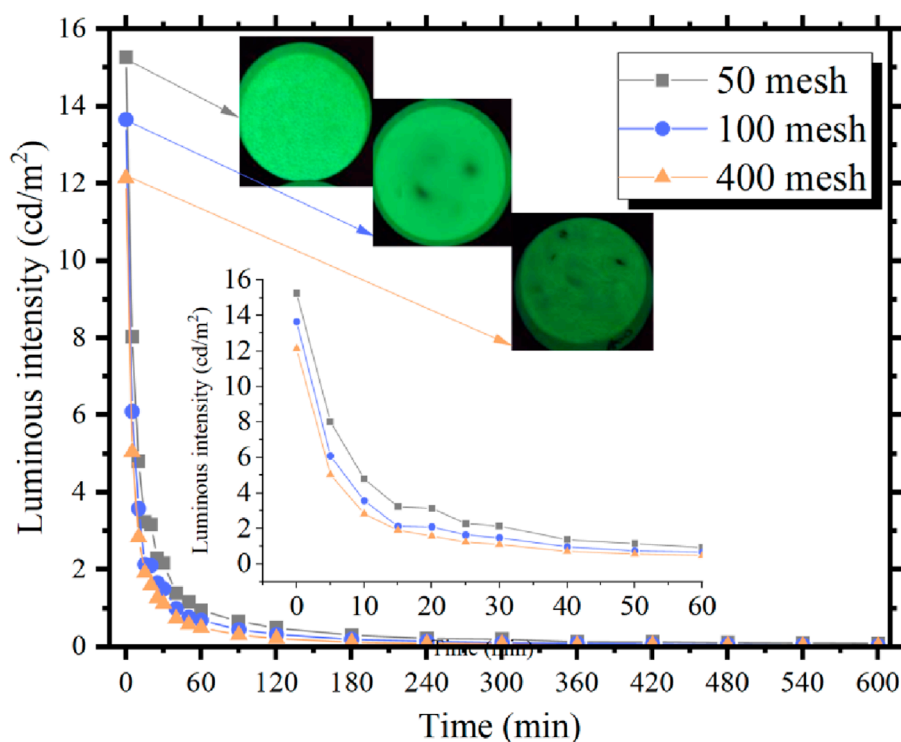


FIGURE 2
Brightness intensity and afterglow decay of the LP.

the duration increased to 6 h, the luminance of the 400 mesh LP particles was undetectable, indicating a significant decline in their afterglow capabilities over time. Furthermore, the disparity in the densities of the LPs and polyurethane resulted in issues such as delamination and segregation during the mixing process. This phenomenon exacerbated with increasing particle sizes, while reduction in the particle sizes to the extreme adversely impacted the mechanical integrity of the material. Taking into account both the luminescent performance and practical conditions of the preparation process, the 100 mesh LP particles (with medium particle sizes) were ultimately chosen as the luminescent material for further testing. This selection was

based on a balanced consideration of the luminance output, stability of the afterglow over time, and mechanical properties of the material. The 100 mesh LP particles offer an optimal combination of these attributes, making them a suitable candidate for applications that require a luminescent material with a prolonged and consistent afterglow as well as robust mechanical performance.

2.1.3 Preparation of polyurethane self-luminous coating

The consistency of the polyisocyanate and polyol within the catalyst mixture is relatively low, and the initial condensation

time for the polyurethane adhesive at ambient temperature is comparatively lengthy. To avoid precipitation of the incorporated LP during curing of the polyurethane adhesive, the adhesive mixture was uniformly heated to 70°C in an oven for 10 min. This preheating step serves to augment the reaction extent between the two components, thereby accelerating the resin curing process and reducing the time required for initial condensation. Following this heating process, the LP was integrated in the adhesive mixture, which was then poured into a standard test mold. The mold was subsequently placed in an oven at 70°C for 5 h to complete the curing process. For each experimental trial, five PSC specimens were fabricated, and their average values were utilized as the representative test results.

A range of six distinct LP doping levels were explored in this study, namely 10 wt%, 20 wt%, 30 wt%, 40 wt%, 50 wt%, and 60 wt%, and these specimens were designated as PSC-1, PSC-2, PSC-3, PSC-4, PSC-5, and PSC-6, respectively. Additionally, a control group comprising polyurethane without LP was established and labeled as PSC-0. To assess the durability of the PSC specimens under environmental stress, ultraviolet and thermal aging tests were conducted, and the corresponding specimens were denoted as PSC-U and PSC-H, respectively.

2.2 Luminescent property measurement

For the experimental evaluations, a screen luminance meter was used to meticulously characterize the luminescence properties of the PSCs. To this end, a selection of artificial light sources that are commonly encountered in nocturnal settings was incorporated in the simulation. These included white fluorescent, red fluorescent, and ultraviolet lamps. The rationale behind this choice is rooted in the understanding that in addition to stimulation by sunlight during the day, the luminescent materials within the PSCs will be activated by illumination from street lamps and vehicular headlights during the nighttime hours. This comprehensive approach ensures that the PSC luminescent performances are thoroughly assessed across a representative range of light sources to provide a more accurate and holistic understanding of the material capabilities for real-world applications.

2.3 Fourier-transform infrared (FTIR) spectrometry

FTIR (NICOLET 6700TM, Semerfly) equipment was used to determine the functional groups of the polyurethane and PSCs. The device had a resolution of 4 cm⁻¹, and the wavenumber was varied in the range of 400–4,000 cm⁻¹.

2.4 Fluorescence microscopy (FM)

To evaluate the surface optical properties of the specimen luminescence, FM (conducted with a MIKON microscope) was used for fluorescence imaging of the PSC surfaces with a magnification of 400×.

2.5 Ultraviolet aging simulations

To better evaluate the durability of the PSCs as pavement surface layer materials, UV aging of the PSC specimens were performed in a UV aging chamber (TIMI880, South Korea) to simulate the conditions encountered by real pavements.

2.6 Fluorescence spectrometry

The photoluminescence spectra (excitation and emission) of the PSC specimens were obtained using the FluoroLog-3 device from HORIBA Instruments Incorporated. A xenon arc lamp was used as the excitation source, and the emission spectra were measured in the wavelength range of 420–700 nm.

2.7 Wear resistance test

Given the intimate contact between the coating and road surface, the material is constantly subjected to cyclic vehicle loads throughout its operational lifespan. The repetitive nature of these loads poses a potential for erosion of the coating material, underscoring the necessity to ascertain its wear resistance. To simulate this wear process, an accelerated loading apparatus known as the model mobile load simulator (MMLS, South Africa) was employed in this study. The test parameters were meticulously calibrated, with the axle load set to 0.7 MPa and tire load set to 0.76 kN. A total of 30,000 test loadings were applied to the specimens to evaluate their performances under controlled conditions. The specimens used in the tests were rutted plate samples with cut-edge dimensions of 300 mm × 200 mm. These rutted plates were categorized into two distinct groups based on their surface treatments: the first group was coated with a primer-marking paint (labeled as PSC-A), and the second group was left uncoated (labeled as PSC-B). The thickness of the PSC applied to each type of rutted plate was systematically varied, with the options being 0.2 kg/m², 0.4 kg/m², 0.6 kg/m², 0.8 kg/m², and 1.0 kg/m². A rutted plate without PSC served as the control group in the experiments. To ensure reliability and reproducibility of the results, each test group was subjected to loading three times.

2.8 Antiflaking test

To quantitatively assess the adhesion between the PSCs and pavement, tensile tests were conducted in accordance with the technical specifications of the coatings. The tensile test is a standard procedure designed to evaluate the bond strength between a coating and its underlying surface; it provides a measure of the force required to dislodge the embedded pull-out specimen from the pavement slab, thereby indicating the adhesive efficacy of the PSC.

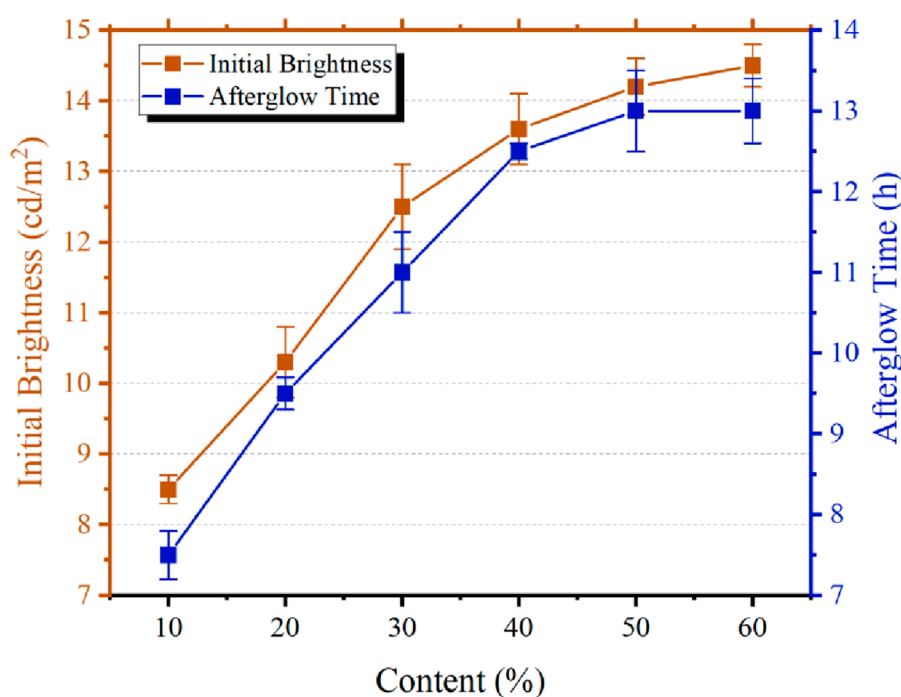


FIGURE 3 Trends showing the effects of LP doping on the luminescence performance of the PSC.

3 Results and discussion

3.1 Factors influencing luminous brightness

3.1.1 LP dosage

It can be seen from Figure 3 that the concentration of the LP particles significantly influences the overall luminescence performance of the PSC. The relationship between the LP content and luminescence intensity typically follows a pattern where increased LP doping levels correspond to enhanced luminescence brightness. Specifically, at an LP doping level of 10%, the PSC exhibits an initial brightness of 8.5 cd/m²; as the LP doping amount increases, there is a discernible positive trend in the initial brightness. This upward trajectory begins to decelerate once the doping level reaches 40%. Upon further increasing the doping to 60%, the initial brightness increases to 14.5 cd/m², representing a substantial 70.58% rise in the luminescence intensity. Furthermore, the afterglow duration of the PSC is markedly affected by the LP doping level. The PSC with 10% LP doping exhibits the shortest afterglow time of 7.5 h; in contrast, the PSC with 60% LP doping produces the longest afterglow duration of up to 13 h. Notably, at an LP doping level of 40%, the afterglow time exhibits no significant change, suggesting that an increase in LP content may lead to saturation at certain luminescent centers or energy levels (Wang et al., 2021a). Once these centers or energy levels reach saturation, an additional increment in the LP content may not result in further brightness enhancement.

To achieve a more nuanced understanding of the luminance variations within the PSCs, comprehensive analyses of the

luminescence spectra were conducted. Figure 4 illustrates the photoluminescence spectra of the PSC specimens with varying LP concentrations. These specimens were uniformly stimulated at a wavelength of 370 nm under identical illumination conditions for a period of 1 h. The data reveal that while the spectra of the specimens with higher LP content had greater intensities, all samples displayed comparable broadband emission profiles, with a peak centered at 513 nm within the green–yellow wavelength range of 450–650 nm. This consistency in spectral shape and positioning suggests that the PSC specimens can absorb UV and visible light, subsequently emitting yellow-green glows. The observed yellow-green luminescence, as depicted in Figure 4, aligns with the characteristic emissions associated with the 4f⁶5d¹–4f⁷ electronic transitions of the Eu²⁺ ions (Wu et al., 2011). This finding is significant as it indicates that the PSC specimens are capable of harnessing UV and visible light to produce luminescent outputs that are perceptible yet within the spectrum of human visual sensitivity. By understanding the relationship between the LP concentrations and resulting photoluminescence spectra, researchers and engineers can optimize the design and fabrication of PSC materials to achieve desired luminance levels and spectral outputs for various practical applications.

As depicted in Figure 5, digital images captured in a dark environment were utilized to evaluate the rate of disintegration of the PSC specimens. It is observed that owing to the phenomenon of luminescence quenching, the PSC specimens demonstrate gradual declines in the macroscale fluctuations of the luminance intensity over time. This pattern of decay is indicative of the temporal evolution of the luminescent properties of the PSC specimens. Upon comparison of the PSC specimens with varying concentrations of

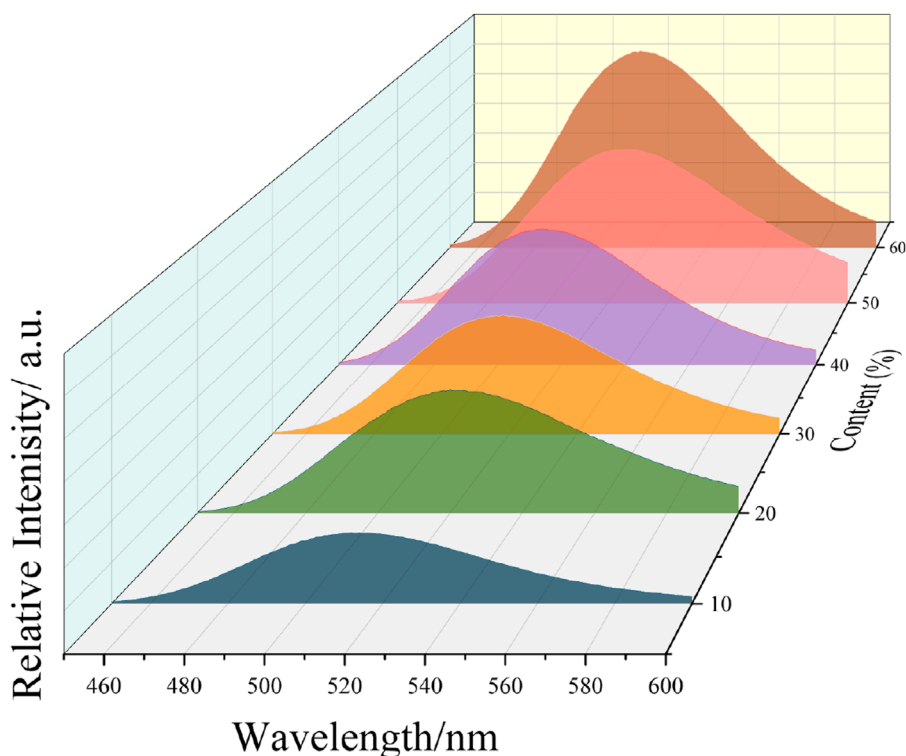


FIGURE 4
Photoluminescence emission spectra of the series of PSCs (excitation wavelength = 370 nm).

the LP material, it was noted that the specimen designated as PSC-6 exhibited the most prolonged decay time and most intense emission. This observation is attributed to the increased energy transfer between the Eu ions present in the specimens for higher LP concentrations, which in turn enhances both the brightness intensity and decay time of the luminescence. However, it is important to recognize that there exists an inherent tradeoff between the decay time and economic considerations in practical applications. Although higher LP doping levels may lead to improved luminescent performances, these are not accompanied by proportional increases in the brightness. Moreover, excess LP concentrations can result in significant increases in the production costs, thereby necessitating balance between performance enhancement and cost-effectiveness.

3.1.2 Coating thickness

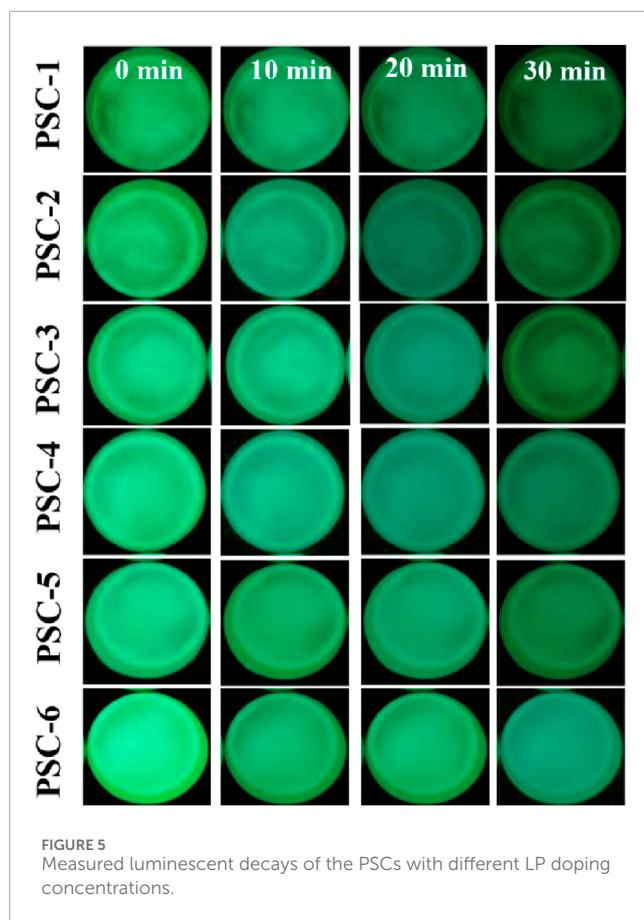
Figure 6 presents a detailed analysis of the impact of coating thickness on the luminescent performance of the PSC. The data indicate that the initial brightness of the PSC is positively correlated with the thickness of the applied coating. Specifically, the initial brightness is observed to be minimal at 11.1 cd/m^2 for a PSC thickness of 0.4 kg/m^2 and reaches a maximum of 14.9 cd/m^2 as the thickness is increased to 1.0 kg/m^2 . It is noteworthy that the rate of increase in the initial brightness of the PSC diminishes significantly when the coating thickness surpasses 0.6 kg/m^2 . This threshold can be interpreted as a critical juncture where the change in brightness is primarily attributed to accumulation of the coating material. This observation is hypothesized to be associated with the arrangement and stacking mode of the luminescent material. As

the coating thickness increases from 0.1 kg/m^2 to 0.6 kg/m^2 , the incremental addition of the LP material predominantly contributes to the enhanced coverage of the mixture surface. However, beyond a certain thickness, the intensity of the excitation light progressively diminishes with increasing depth of penetration, ultimately failing to sufficiently excite the lower layers of the material. Despite this trend, the LP material forms an internal luminous mass with light transmission to the adjacent material that does not surpass the threshold required for stable luminescence.

Furthermore, the coating thickness exerts minimal influence on the afterglow duration, with the difference between the longest and shortest afterglow times being a mere 1.5 h. Consequently, considering both economic factors and luminous efficiency, the optimal PSC thickness is identified to be 0.6 kg/m^2 , striking a balance between cost and performance.

3.1.3 Excitation time

The excitation reaction of a luminescent material is recognized as an energy storage phenomenon, which implies that the duration of excitation plays a pivotal role in shaping the luminescent characteristics of the coating (Lyu et al., 2020). It has been established that there exists a saturation point in the excitation process, beyond which further exposure to light does not enhance the luminescence performance of the PSC (Lin et al., 2023). The present investigation aims to ascertain the specific excitation saturation times for the PSC subjected to various types of light sources. This inquiry is significant as it seeks to delineate the optimal excitation conditions necessary to maximize the luminescent



efficacy of the PSC. By identifying the saturation point, it is feasible to regulate the excitation process, thereby ensuring that the PSC achieves its highest potential in terms of luminescence output without unnecessary overexposure. Moreover, understanding the excitation saturation times for different light sources provides valuable insights that can guide the practical applications and maintenance of PSCs.

Figure 7 presents a comparative analysis of the initial brightness of the PSC specimens under the influence of different excitation light sources and varying exposure durations. The data clearly delineate that specimens excited by sunlight exhibit notably lower initial brightness after 5 min of exposure than those excited by the other types of light sources. However, it is observed that the sunlight-excited specimens demonstrate more pronounced rates of increase in initial brightness with extended excitation times. Upon reaching 15 min of exposure, the rate of increase in the initial brightness for the sunlight-excited specimens begins to decelerate; after an exposure duration of 20 min, these specimens achieve the highest initial brightness among the four groups. The luminescence performances of the specimens excited by white and yellow fluorescent lamps appear to be relatively analogous across various aspects, with the initial brightness stabilizing after 15 min of excitation.

Notably, the specimens excited by UV light exhibit the steepest initial brightness increase, with a 45.4% enhancement within the initial 5-min period. The brightness of these specimens continues to escalate at 10 min before reaching a stable state, indicating that UV

light possesses superior excitation efficiency for the PSC specimens. As the duration of excitation increases, the initial brightness of the specimens reaches an optimal state, implying that UV light, specifically that in the 10–400 nm wavelength range, is the most effective excitation source among the components of natural light for light-emitting properties of the PSCs.

3.1.4 RP dosage

RPs play pivotal roles in the optical performances of coatings by scattering and diffusing any incident light throughout the material. This scattering effect facilitates the propagation and distribution of light within the coating, thereby enhancing the brightness and uniformity of the surface of the PSC. The incorporation of RPs into the coating also serves to augment its transparency, enabling more light to penetrate and excite the luminescent material at the coating's base. This, in turn, amplifies the self-luminous effect of the PSC. The luminescence performance of the PSC is influenced by the amount of RP incorporated, necessitating the determination of an optimal RP dosage through a series of tests with varying RP ratios. In the experimental procedure, the PSC specimens were fabricated with a standard thickness of 0.6 kg/m^2 and fixed LP concentration of 60%. The RP doping levels were then systematically varied at 0%, 10%, 20%, 30%, 40%, 50%, and 60%. Following preparation, the specimens were subjected to a 20 h period of darkness to precondition the luminescent material. Subsequently, the specimens were exposed to a UV lamp for 10 min to induce excitation of the luminescent particles. The luminous brightness of each specimen was then assessed after a 1-h interval to allow observation of the luminance trends under different RP doping conditions.

Figure 8 illustrates the luminance variations of the PSCs as functions of different RP doping levels. The data indicate that the incorporation of RPs can markedly enhance the luminous brightness of the PSCs, with an increase of 0.042 cd/m^2 observed at the 10% RP doping level. However, a discernible trend of diminishing luminance intensity is noted with progressive increment in the RP doping concentration. A schematic representation of the luminescence mechanism within the PSC is provided in Figure 9. The underlying hypothesis here is that an increase in the RP density may necessitate the passage of additional beams, effectively prolonging the distance traveled by the light within the coating. This extended path may result in the attenuation of light, consequently diminishing the luminescence of the coating. Furthermore, while the RP is instrumental in scattering light, excess concentration of the powder could lead to excessive light scattering. This overscattering may cause multiple internal reflections of the light within the coating, resulting in loss of directionality and culminating in reduction of the overall brightness of the coating. This phenomenon may also contribute to blurred or uneven distribution of luminescence across the coating surface.

Based on these findings, the optimal RP doping level was determined to be 10%. Regarding the luminescent properties of the PSC, the recommended formulation for the material mix was established as 60% doping with the LP material, coating thickness of 0.6 kg/m^2 , and 10% doping with the RP. This combination is anticipated to yield a PSC with balanced luminance characteristics and optimal visual performance, ensuring the practicality and effectiveness of the self-luminous coating in relevant applications.

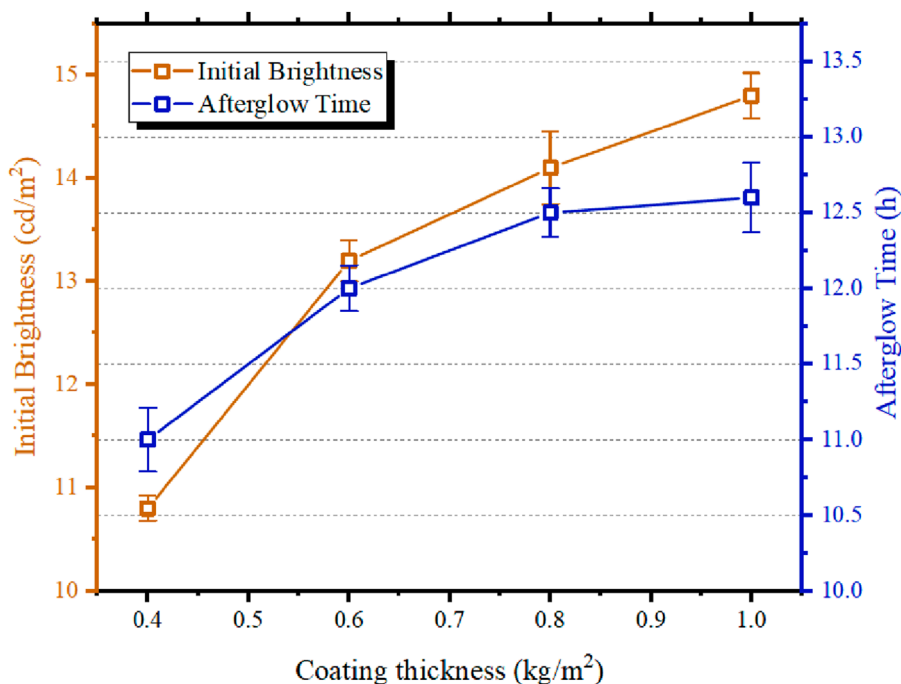


FIGURE 6 Effects of luminescent coating thickness on the luminescent properties of the PSC.

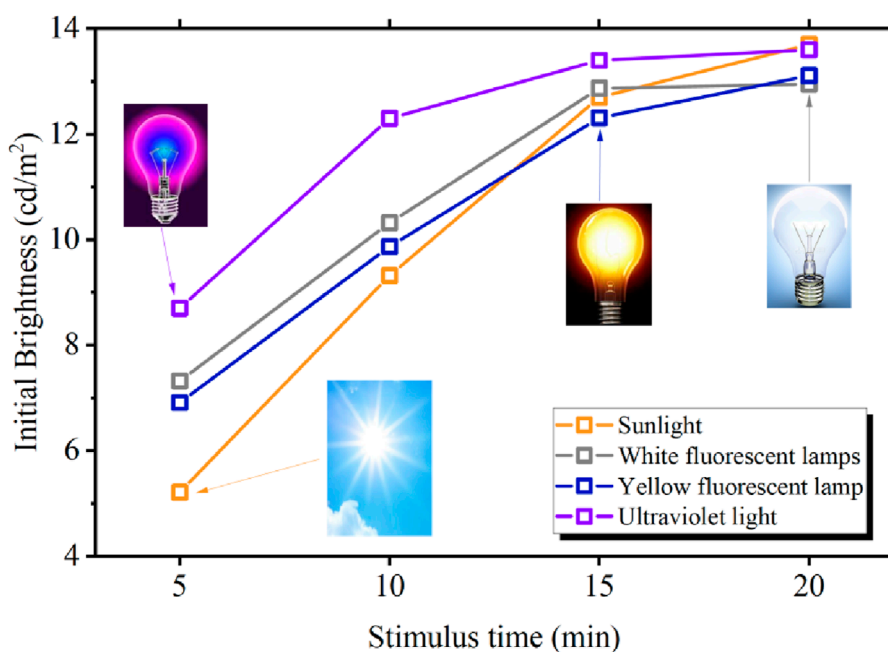


FIGURE 7 Trends showing the effects of excitation time and light source type on the luminescence performance of the PSC.

3.2 Chemical stability

The emergence of novel or characteristic peaks within a spectrum is often indicative of chemical reactions between the

component materials. To investigate the nature of the interactions between the LP particles and polyurethane, FTIR analyses were conducted on the various PSC specimens, and these results are graphically depicted in Figure 10. As observed in Figure 10, the

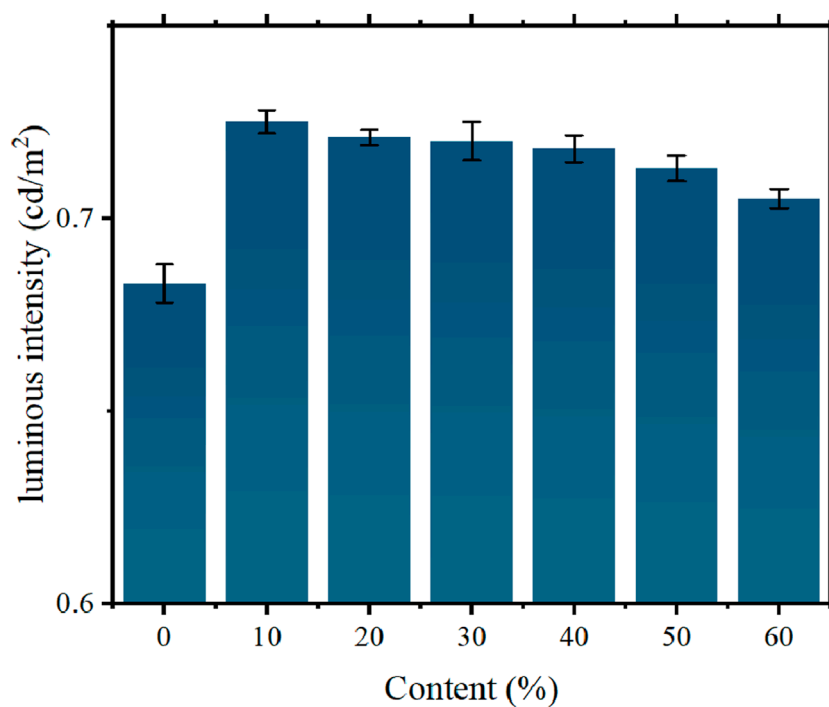


FIGURE 8
Effects of different doping levels of RP on the luminescence brightness after 1 h.

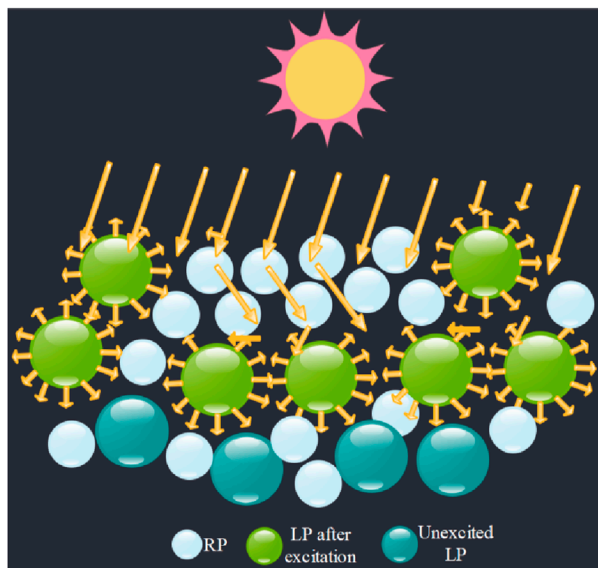


FIGURE 9
Schematic diagram of transmission in the optical medium and excitation inside the PSC.

infrared spectra of the different PSC specimens, irrespective of LP doping, exhibited identical peak shapes. The absence of new absorption peaks suggests that the combination of the LP and urethane did not result in the formation of new substances, thereby indicating that the process is purely physical mixing. Nevertheless,

variations in the LP doping levels were accompanied by discernible alterations in the absorption peak intensities. Specifically, the C-H stretching vibration on the saturated carbon was detected at $2,923\text{ cm}^{-1}$; carbonyl-C=O stretching vibration was observed at $1,726\text{ cm}^{-1}$; double-bond stretching vibration or benzene ring skeleton vibration was identified at $1,525\text{ cm}^{-1}$; C=N, C=C, N=N, and N=O double-bond stretching vibrations or benzene ring skeleton vibrations were noted at $1,216\text{ cm}^{-1}$; and C-H in-plane bending vibration was observed at $1,043\text{ cm}^{-1}$. The intensities of these vibrations were found to be inversely related to the LP doping levels.

The above observations imply that incorporation of the luminescent material induced modifications in certain components of the urethane material species, such as alterations in the lattice structure and escalation in the intensities of the vibrations associated with crystal defects (Li et al., 2021). These findings are instrumental in understanding the interactions between the LP particles and polyurethane matrix, providing insights that can guide the development of PSC materials with enhanced luminescent properties and structural stabilities.

3.3 Antiaging properties

The applications of polyurethane materials are often accompanied by the tendency for transparent polyurethane to exhibit yellowing upon exposure to light, oxygen, and UV radiation. This discoloration is attributed to the aging phenomenon. To elucidate the antiaging characteristics of the PSCs, Figure 11 presents the pre- and post-aging FTIR plots of the PSC-0 and

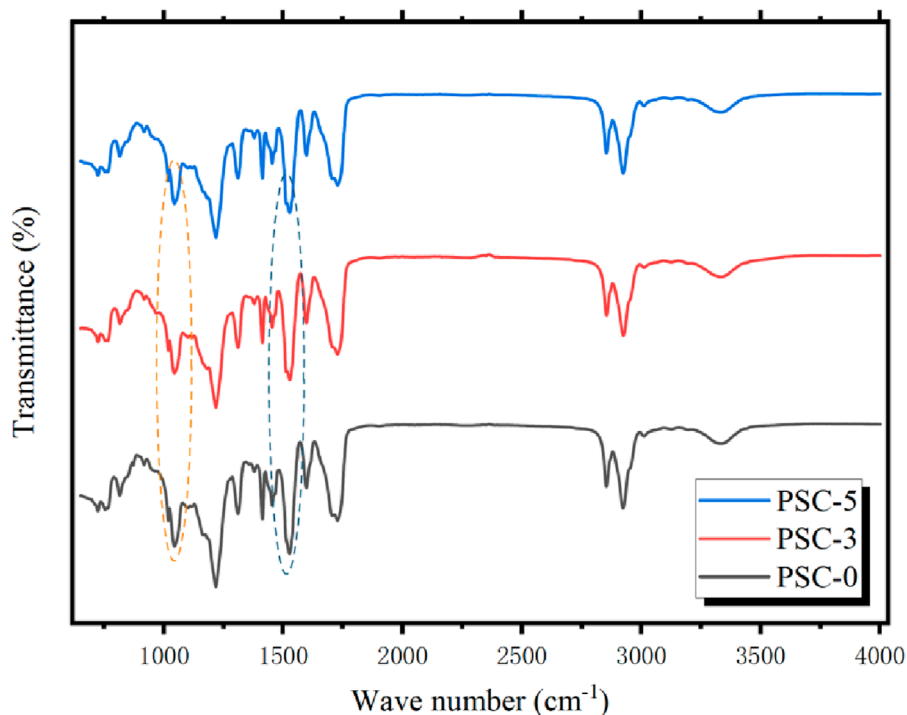


FIGURE 10
Infrared transmittance spectra of different PSCs.

PSC-30 specimens. The analysis reveals that regardless of the aging process being photoinduced or thermally induced, the infrared spectral patterns and peak profiles remain consistent before and after aging. The absence of new absorption peaks further indicates that the discolorations associated with light and thermal aging in polyurethane are not caused by the formation of new chemical species. However, the aging process results in intensity variations of the absorption peaks of the polyurethane material. For instance, the O-H stretching vibration at $3,334\text{ cm}^{-1}$, carbonyl-C=O stretching vibration at $1,726\text{ cm}^{-1}$, and C-H out-of-plane bending vibrations of olefins and aromatic hydrocarbons at 753 cm^{-1} exhibit enhanced peak intensities post-aging compared to their pre-aging counterparts.

The FTIR spectrum of the light-aged PSC-0U specimen demonstrates a significantly pronounced peak profile than that of the thermally aged PSC-0H. This distinction underscores the differential impacts of aging mechanisms on the material's spectral characteristics, providing insights into the resilience of PSC materials against environmental degradation.

Subsequent analyses of the PSC specimens after the light and thermal aging treatments indicate that the infrared spectra remain consistent with those of the untreated specimens. This finding suggests that neither light nor thermal aging induced formation of new chemical entities within the specimens. However, it is important to highlight that the capacity of a specimen to absorb infrared radiation is notably diminished following the aging processes. This reduction is primarily evident in the attenuation of the absorption peaks, with the light-aged specimens exhibiting more pronounced decreases in absorption than the thermally aged specimens. This

observed reduction in the infrared absorption capacity may be ascribed to alterations in the material's crystal structure during the aging process. These structural modifications may also encompass the emergence of lattice defects and variations in crystal size (Boubakri et al., 2010a; Ge et al., 2016). Such changes in the crystal architecture can modulate the intensities of the vibrational modes, affecting the relative magnitudes of the peaks observed in the FTIR spectra. Furthermore, the presence of dopants within the material influences the vibrational modes of the constituent molecules, resulting in shifts in the peak positions (Ge et al., 2016). This disruption predominantly occurs at the surface of the material, compromising the intermolecular linkages that hold the structure together (Boubakri et al., 2010b).

3.4 Wear resistance

Figure 12 delineates the mass loss of the PSC specimen after 30,000 cycles of small, accelerated loading tests. The data unequivocally demonstrate the efficacy of the PSC in significantly attenuating the mass loss of the specimen. This reduction is attributed to the coating material's ability to form a protective layer on the preexisting asphalt mixture, thereby prioritizing tire abrasion on the coating itself. The PSC's superior adhesion characteristics are instrumental in effectively withstanding these abrasive forces exerted by tire contact. Furthermore, an analysis of the mass loss in relation to the PSC thickness reveals an initial sharp decline followed by stabilization. Notably, when compared to the uncoated control specimen, the application of a PSC of thickness 0.4 kg/m^2

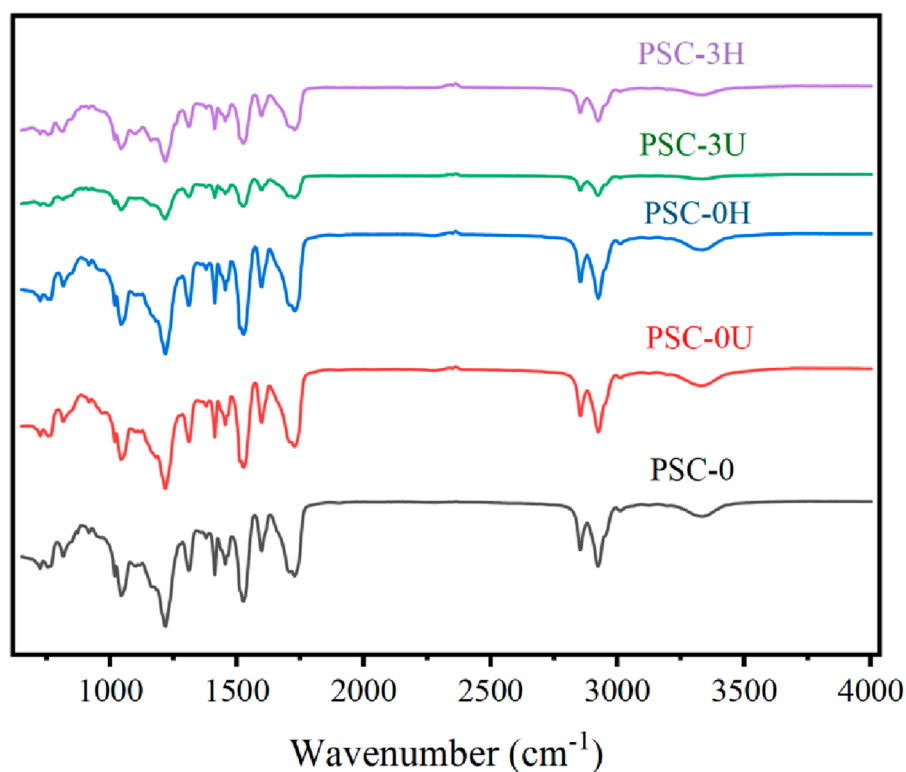


FIGURE 11
FTIR spectra of the plain polyurethane coating and PSC-30 before and after aging.

resulted in a 52.9% reduction in the mass loss, while a 1.0 kg/m^2 coating thickness led to a 35.3% reduction in the mass loss relative to the control group. This phenomenon can be rationalized by considering the incremental protective effects provided by the PSC with increasing quantity of the material.

The rationale behind this phenomenon is the progressive nature of the protective film formed by the PSC with increasing material quantities. At a coating thickness of 1.0 kg/m^2 , the PSC may not uniformly envelop the mixture, with the majority of the coating being concentrated within the surface grooves of the rutted plate. This distribution limits the coating's ability to serve as an effective antiwear barrier. However, as the PSC thickness is increased, the interaggregate grooves are progressively filled with the coating material; this filling enhances the material's capacity to resist abrasion, leading to a pronounced initial decrease in the mass loss. Ultimately, as the coating dosage increases, the mass loss reaches a plateau, reflecting the optimal coating thickness for maximizing the protective benefits and minimizing the material wear.

Supplementary investigations into specimens coated with a primer have yielded noteworthy outcomes. It was observed that the group of specimens precoated with marking paints exhibited a significantly lower mass loss than the uncoated group, with reductions ranging from approximately 33.4%–47.1%. This enhancement in durability is attributed to the primer's role in preemptively filling the microgrooves present on the road surface. By doing so, the primer augments the efficiency of the luminous coating material in safeguarding the underlying mixture. Under the effect of

vehicular traffic, deformations by tires can induce a “pump suction” effect on the road surface. In such instances, if the bond strength between the PSC and road surface is inferior to the suction force generated by the “pump suction” phenomenon, the coating is prone to spalling (Li B. et al., 2023). The application of primer-marking coatings can effectively ameliorate the bonding characteristics of asphalt mixture surfaces. This improvement in adhesion is crucial for minimizing the incidence of surface peeling of the light-emitting functional layer.

The utilization of primer-marking paints in the coating process is therefore a strategic intervention that bolsters the integrity and longevity of the PSC. By enhancing the interface between the coating and road surface, the primer contributes to the overall durability and performance of the SLP system, ensuring that it remains effective and visually intact under dynamic vehicular traffic conditions.

3.5 Antipeeling resistance

The incorporation of the LP and RP in the PSC presents the potential for formation of a weak layer at sites where these components are clustered. Such areas may exhibit suboptimal adhesion, leading to flaking and consequently compromised luminescence effects. This phenomenon is further influenced by the “precipitation” tendency of the luminescent material (Wang et al., 2021b), which suggests that increases in the coating thickness cause greater accumulation of the luminescent material at the coating's base. This accumulation can subsequently impact the

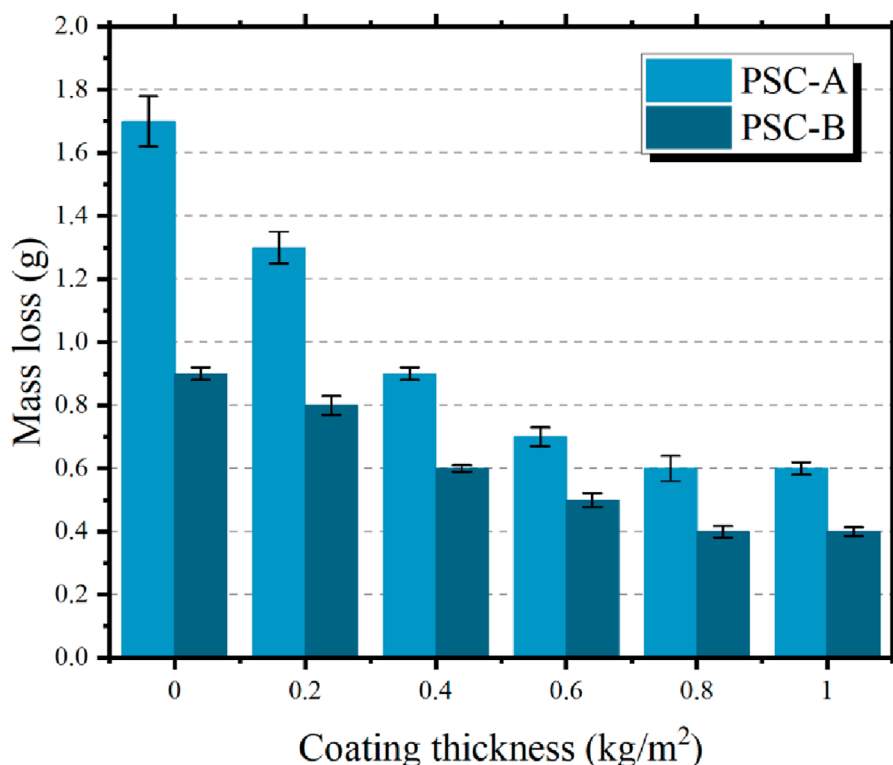


FIGURE 12
Mass loss of the PSC specimen subsequent to small, accelerated loading tests.

material's resistance to flaking. Figure 13 visually represents the anti-peeling test results, which were instrumental in quantifying the influence of coating thickness on the PSC's propensity to resist peeling.

Figure 13 presents a detailed analysis of the relationship between the coating thickness and tensile strength of the PSC as well as its resistance to flaking, irrespective of the presence of primer-marking paint. The tensile strength of the PSC-A coating, for instance, was measured to be 5.4 MPa for a thickness of 0.4 kg/m². However, upon increasing the thickness to 0.8 kg/m², the tensile strength dropped below 5 MPa. This pronounced reduction in the tensile strength is likely attributable to the formation of an internally mechanically weak layer within the coating. As the thickness of the PSC coating increases, the potential for the development of larger stress concentration areas within the pavement structure increases. Thicker coatings are more susceptible to accumulation of internal stresses when exposed to external loads or temperature fluctuations, which can precipitate localized areas of bond weakness. Furthermore, the increase in coating thickness may induce alterations in the material properties of the PSC, such as disparities in the internal hardness and elastic modulus, owing to the distribution of the LP material. These variations can result in uneven stress distribution between the coating and road surface, adversely affecting the bond integrity.

In light of these observations, it is recommended that the thickness of the PSC be maintained within 0.6 kg/m² for practical applications. This optimal thickness range ensures a balance between the coating's mechanical strength and its resistance to flaking,

thereby enhancing the overall durability and performance of the PSC in real-world scenarios.

An examination of the tensile properties of PSC-B reveals a noteworthy trend. Contrary to expectations, the increase in coating thickness did not result in marked reduction in the bond strength. Even at a thickness of 0.8 kg/m², the PSC-B coating sustained a tensile strength of 5.8 MPa, which was a 26.1% improvement over the tensile strength of the uncoated PSC. This observation suggests that the primer-marking paint possesses certain inherent advantages that contribute to its superior performance. The primer-marking paint typically exhibits certain degrees of elasticity and flexibility, which enable it to accommodate the minor deformations and vibrations characteristic of road surfaces. This adaptability can mitigate the fatigue damage to the coating, thereby enhancing its tensile strength. Moreover, primer-marking paints have been recognized for their exceptional adhesion properties, ensuring strong bonds with pavement surfaces. The application of the primer-marking paint thus fortifies the adhesion between the coating and pavement, reducing the likelihood of delamination of the PSC from the pavement. This, in turn, bolsters the overall tensile strength of the system.

In light of these findings, it is advisable that the luminous functional coating be applied in a two-tiered approach in practical applications, with the primer-marking paint being applied to the lower layer. This strategy ensures a robust and durable coating system that is well-equipped to withstand the demands of long-term use, thereby fulfilling the requirements for durability and performance in real-world settings.

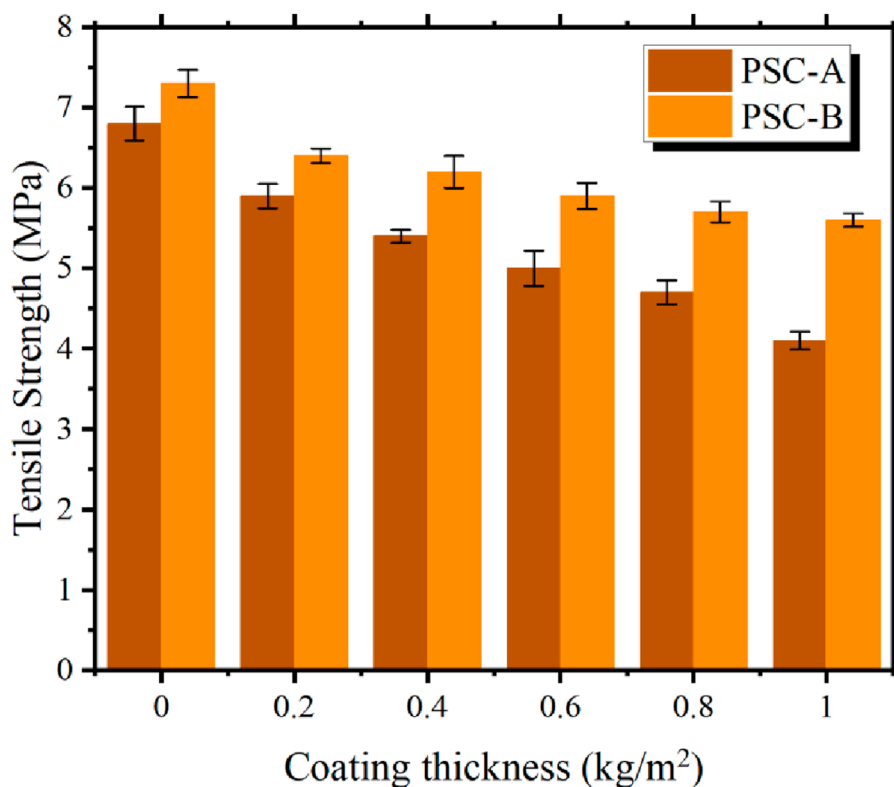


FIGURE 13
Effects of coating thickness on the antiflaking resistance.

4 Conclusion

In the present investigation, PSCs were fabricated by utilizing polyurethane as the primary film-forming substance complemented by LP and RP as the secondary film formers. This work encompassed a comprehensive evaluation of the material composition, with examination of its indoor afterglow properties, resistance to aging, endurance against wear, and performance against flaking. The findings thus lead to the following conclusions:

- (1) The higher the amount of LP doping, the better is the luminescence performance of the PSC; when the doping amount reaches 60%, the initial brightness reaches 14.5 cd/m^2 , which is a 70.58% increase in brightness over that of the control group. When the PSC thickness increases, the luminous brightness trend progressively reduces and nearly stops expanding beyond 0.6 kg/m^2 ; this is related to the excitation conduction path of the PSC.
- (2) In the context of luminescent material excitation, UV radiation has superior efficiency to white and yellow light sources. The PSC exhibits maximal responsiveness to UV light, specifically in the wavelength range of 10–400 nm. Furthermore, the optimal luminance of the PSC is achieved with an LP doping level of 10%. Beyond this threshold, an excess concentration of RP is observed that compromises the effective excitation efficiency of the incident light, thereby impacting the luminescent output of the PSC.

- (3) The mixing of polyurethane materials with LP is a simple physical co-mingling, and there is no creation of new substances; however, the number of functional groups connecting the molecules is obviously reduced.
- (4) The application of primer-marking coatings can significantly enhance the abrasion resistances of PSCs. The mass loss of a PSC of thickness 0.4 kg/m^2 is reduced to 52.9% of that of a specimen without primer-marking coating. Upon incrementing the coating thickness, the tensile strength of the PSC declines gradually, which concomitantly results in decreased peeling resistance irrespective of the presence of the primer-marking paint. To optimize the performance and durability of a PSC in practical applications, it is recommended to maintain the coating thickness below 0.6 kg/m^2 , thereby achieving a balance between mechanical strength and resistance to delamination.

5 Recommendations for future work

PSCs are potentially innovative materials for improving transportation safety. The following are some directions for future research. Further optimization of the PSCs can improve road visibility at night, thereby improving traffic safety; this may include improving the coating brightness, color vibrancy, and performance under various weather conditions. PSCs adapted to different weather conditions, including extreme heat, cold, rain, and snow, are

also a possible avenue of investigation, which can help ensure that the coatings maintain consistent performance under various environments.

Data availability statement

The raw data supporting the conclusion of this article will be made available by the authors without undue reservations.

Author contributions

QL: conceptualization, data curation, investigation, and writing–review and editing. XL: formal analysis, methodology, and writing–original draft. ZL: resources, software, and writing–original draft. KL: validation and writing–original draft.

Funding

The author(s) declare that financial support was received for the research, authorship, and/or publication of this article. This

References

- Bacero, R., To, D., Arista, J. P., Cruz, M. K. D., Villaneva, J. P., and Uy, F. A. (2015). Evaluation of strontium aluminate in traffic paint pavement markings for rural and unilluminated roads. *J. East. Asia Soc. Transp. Stud.* 11, 1726–1744. doi:10.11175/easts.11.1726
- Bashir, M. S., Kong, X. Z., Ramzan, N., Arif, M., Bashir, H., Azhar, U., et al. (2022). Systematic study on interfacial polymerization mechanism of toluene diisocyanate and water for the preparation of polyurea microspheres. *Inorg. Chem. Commun.* 143, 109814. doi:10.1016/j.inoche.2022.109814
- Bi, Y., Pei, J., Chen, Z., Zhang, L., Li, R., and Hu, D. (2021). Preparation and characterization of luminescent road-marking paint. *Int. J. Pavement Res. Technol.* 14 (2), 252–258. doi:10.1007/s42947-020-0229-3
- Boubakri, A., Guermazi, N., Elleuch, K., and Ayedi, H. F. (2010b). Study of UV-aging of thermoplastic polyurethane material. *Mater. Sci. Eng. A* 527 (7), 1649–1654. doi:10.1016/j.msea.2010.01.014
- Boubakri, A., Haddar, N., Elleuch, K., and Bienvenu, Y. (2010a). Impact of aging conditions on mechanical properties of thermoplastic polyurethane. *Mater. Des.* 31 (9), 4194–4201. doi:10.1016/j.matdes.2010.04.023
- Bredol, M., Kynast, U., and Ronda, C. (1991). Designing luminescent materials. *Adv. Mater.* 3 (7-8), 361–367. doi:10.1002/adma.19910030707
- Del Serrone, G., Peluso, P., and Moretti, L. (2023). Photovoltaic road pavements as a strategy for low-carbon urban infrastructures. *Heliyon* 9 (9), e19977. doi:10.1016/j.heliyon.2023.e19977
- Dong, S., Zhang, W., Wang, X., and Han, B. (2023). New-generation pavement empowered by smart and multifunctional concretes: a review. *Constr. Build. Mater.* 402, 132980. doi:10.1016/j.conbuildmat.2023.132980
- Falchetto, A. C., Moon, K. H., Wang, D., and Riccardi, C. (2018). Investigation on the cooling medium effect in the characterization of asphalt binder with the bending beam rheometer (BBR). *Can. J. Civ. Eng.* 45 (7), 594–604. doi:10.1139/cjce-2017-0586
- Fang, G., Zhaoxian, X., Hao, X., and Yongxi, L. (2009). Improved performance of strontium aluminate luminous coating on the ceramic surface. *J. Phys. Conf. Ser.* 152 (1), 012082. doi:10.1088/1742-6596/152/1/012082
- Gao, S., Wang, M., Tang, Z., and Tang, A. (2013). Cause of enhancement of the coating wear resistance by luminescent material SrAl₂O₄: Eu²⁺. *New Build. Mater.* 40 (10), 62–65.
- Ge, Y.-H., Kang, J.-Y., Zhou, J.-H., and Shi, L.-W. (2016). Theoretical investigation on thermal aging mechanism and the aging effect on mechanical properties of HTPB–IPDI polyurethane. *Comput. Mater. Sci.* 115, 92–98. doi:10.1016/j.commatsci.2015.12.050

work was supported by the Foundation of Guizhou Provincial Education Department for Youth (Qianjiaoj, grant no. [2022]154) and Natural Science Foundation of Guizhou Minzu University (grant no. GZMUZK [2023] YB08).

Conflict of interest

The authors declare that the research was conducted in the absence of any commercial or financial relationships that could be construed as a potential conflict of interest.

Publisher's note

All claims expressed in this article are solely those of the authors and do not necessarily represent those of their affiliated organizations, or those of the publisher, the editors, and the reviewers. Any product that may be evaluated in this article, or claim that may be made by its manufacturer, is not guaranteed or endorsed by the publisher.

- Guo, R., and Liu, S. (2022). Design and experiment of self-luminescent asphalt-based pavement materials. *Constr. Build. Mater.* 342, 127991. doi:10.1016/j.conbuildmat.2022.127991

- Hai, O., Ren, Q., Wu, X., Zhang, Q., Zhang, Z., and Zhang, Z. (2019). Insights into the element gradient in the grain and luminescence mechanism of the long afterglow material Sr₂MgSi₂O₇: Eu²⁺, Dy³⁺. *J. Alloys Compd.* 779, 892–899. doi:10.1016/j.jallcom.2018.11.163

- Li, B., Zhang, P., Zhu, X., Wei, D., and Li, Q. (2023b). Permeability model and characteristics analysis of porous asphalt mixture under the circulation clogging and cleaning. *Road Mater. Pavement Des.* 24 (6), 1440–1460. doi:10.1080/14680629.2022.2075788

- Li, P., Yang, T., Ma, P., Fei, X., Li, F., Ye, J., et al. (2023a). Luminous and bonding performance of self-luminescent cementitious coatings based on white cement and geopolymer. *Constr. Build. Mater.* 362, 129814. doi:10.1016/j.conbuildmat.2022.129814

- Li, Q., Wang, T., Jin, R., Zhou, H., Zhang, H., Ni, T., et al. (2021). Study on preparation and properties of energy-storing self-luminous plastics. *Energy Rep.* 7, 559–565. doi:10.1016/j.egy.2021.10.006

- Lin, H., Chen, F., and Zhang, H. (2023). Active luminous road markings: a comprehensive review of technologies, materials, and challenges. *Constr. Build. Mater.* 363, 129811. doi:10.1016/j.conbuildmat.2022.129811

- Lyu, L., Chen, Y., Yu, L., Li, R., Zhang, L., and Pei, J. (2020). The improvement of moisture resistance and organic compatibility of SrAl₂O₄: Eu²⁺, Dy³⁺ persistent phosphors coated with silica–polymer hybrid shell. *Materials* 13 (2), 426. doi:10.3390/ma13020426

- Mierlo, M. v. (2017) *An exploration of the potential of light emitting road marking.*

- Okimura, K., Mian, M. S., Yamaguchi, I., and Tsuchiya, T. (2023). High luminous transmittance and solar modulation of VO₂-based smart windows with SiO₂ anti-reflection coatings. *Sol. Energy Mater. Sol. Cells* 251, 112162. doi:10.1016/j.solmat.2022.112162

- Pan, P., Li, Y., Chen, Y., Shu, S., Hu, X., and Wang, N. (2023). Design and performance evaluation of the epoxy-based self-luminous pavement marking. *Case Stud. Constr. Mater.* 19, e02477. doi:10.1016/j.cscm.2023.e02477

- Poulikakos, L. D., Pasquini, E., Tusar, M., Hernando, D., Wang, D., Mikhailenko, P., et al. (2022). RILEM interlaboratory study on the mechanical properties of asphalt mixtures modified with polyethylene waste. *J. Clean. Prod.* 375, 134124. doi:10.1016/j.jclepro.2022.134124

- Praticò, F. G., Vaiana, R., and Noto, S. (2018). Photoluminescent road coatings for open-graded and dense-graded asphalts: theoretical and experimental investigation. *J. Mater. Civ. Eng.* 30 (8), 04018173. doi:10.1061/(asce)mt.1943-5533.0002361

- Sayles, C., Finnegan, N., Pike, T., and Spence, M. W. (2022). Toluene diisocyanate occupational exposure data in the polyurethane industry (2005–2020): a descriptive summary from an industrial hygiene perspective. *Toxicol. Industrial Health* 38 (9), 606–621. doi:10.1177/07482337221112225
- Schupp, T., and Plehiers, P. M. (2022). Absorption, distribution, metabolism, and excretion of methylene diphenyl diisocyanate and toluene diisocyanate: many similarities and few differences. *Toxicol. Industrial Health* 38 (9), 500–528. doi:10.1177/07482337211060133
- Sha, A., Liu, Z., Jiang, W., Qi, L., Hu, L., Jiao, W., et al. (2021). Advances and development trends in eco-friendly pavements. *J. Road Eng.* 1, 1–42. doi:10.1016/j.jreng.2021.12.002
- Villa, C., Brémond, R., Eymond, F., and Saint-Jacques, E. (2022). Characterization of luminescent road markings. *Light. Res. Technol.* 55 (4-5), 459–473. doi:10.1177/14771535221111052
- Walther, A., Büchler, S., Cannone Falchetto, A., Wang, D., Riccardi, C., and Wistuba, M. P. (2019). Experimental investigation on asphalt mixtures prepared with reclaimed asphalt pavement and rejuvenators based on the BTSV method. *Road Mater. Pavement Des.* 20 (7), 1695–1708. doi:10.1080/14680629.2019.1594053
- Wang, K., Lu, Z., Zou, Y., Zhu, Y., and Yu, J. (2023b). Preparation and performance characterization of an active luminous coating for asphalt pavement marking. *Coatings* 13 (6), 1108. doi:10.3390/coatings13061108
- Wang, W., Jiao, W., Sha, A., Li, X., Jiang, W., and Yuan, D. (2023a). Study on the mechanics and functionalities of self-luminous cement-based materials with energy storage and slow release properties. *Sol. Energy* 259, 72–85. doi:10.1016/j.solener.2023.04.049
- Wang, W., Sha, A., Falchetto, A. C., Wang, D., Jiang, W., and Li, X. (2022a). Properties analysis of self-luminous cement-based materials with different colors and their visual comfort evaluation on pavement. *Sol. Energy* 247, 214–227. doi:10.1016/j.solener.2022.10.013
- Wang, W., Sha, A., Li, X., Zhang, F., Jiang, W., Yuan, D., et al. (2022b). Water resistance and luminescent thermal stability of SiO₂ coated phosphor and self-luminous cement-based materials: view from the perspective of hydration balance. *Constr. Build. Mater.* 319, 126086. doi:10.1016/j.conbuildmat.2021.126086
- Wang, W., Sha, A., Lu, Z., Jia, M., Jiang, W., Liu, Z., et al. (2021b). Self-luminescent cement-based composite materials: properties and mechanisms. *Constr. Build. Mater.* 269, 121267. doi:10.1016/j.conbuildmat.2020.121267
- Wang, W., Sha, A., Lu, Z., Yuan, D., Jiang, W., and Liu, Z. (2021a). Cement filled with phosphorescent materials for pavement: afterglow decay mechanism and properties. *Constr. Build. Mater.* 284, 122798. doi:10.1016/j.conbuildmat.2021.122798
- Wei, J., Ling-qiang, B., Bo, Z., Wang-jie, W., and Ai-min, S. (2022). Design and properties of epoxy-based self-luminous road materials. *China J. Highw. Transp.* 35 (7), 67.
- Wu, H., Hu, Y., Chen, L., and Wang, X. (2011). Investigation on the enhancement and the suppression of persistent luminescence of Re³⁺ doped Sr₂EuMgSi₂O₇ (Re=Dy, Yb). *J. Alloys Compd.* 509 (11), 4304–4307. doi:10.1016/j.jallcom.2011.01.051
- Yuanshuai, D., Yunxue, H., and Zhong, J. (2020). Research on compatibility of energy storage luminescent materials based on road safety. *Highway* 2 (5), 272–280.
- Zheng, M., Li, X., Bai, Y., Tang, S., Li, P., and Zhu, Q. (2023). Sunlight-activated long persistent luminescent coating for smart highways. *Coatings* 13 (6), 1050. doi:10.3390/coatings13061050